Available online at www.sciencedirect.com

ScienceDirect

International Journal of Solids and Structures 43 (2006) 6309–6325

INTERNATIONAL JOURNAL OF SOLIDS and STRUCTURES

www.elsevier.com/locate/ijsolstr

End reflections in a layered piezoelectric circular cylinder

H. Bai [a], A.H. Shah [b], S.B. Dong [c,*], E. Taciroglu [c]

[a] *Lakehead University, Thunder Bay, Ont., Canada*
[b] *The University of Manitoba, Winnipeg, Man., Canada*
[c] *Department of Civil and Environmental Engineering, University of California, Los Angeles, 2066 Engineering I, Los Angeles, CA 90095-1593, USA*

Received 31 May 2005
Available online 4 October 2005

Abstract

End reflection phenomenon in a semi-infinitely long layered piezoelectric circular cylinder is constructed with modal data from a spectral decomposition of the differential operator governing its natural vibrations. These modal data consist of all propagating modes and edge vibrations and they constitute the basis for a wave function expansion of the reflection of waves arriving at the traction-free end of the cylinder. Without any other external stimulus, a passive reflection event occurs. This traction-free end condition is enforced at the Gaussian integration points over the end cross-section on the combination of incoming and reflected wave fields. Reflections due to monochromatic incoming axisymmetric ($m = 0$) and flexural ($m = 1$) waves are studied and two numerical examples are presented.

For an incoming axisymmetric wave, there is a particular frequency that induces an end resonance, which is characterized by high (but finite) amplitudes of end displacements vis-a-vis those of neighboring (i.e., slightly different) frequencies. This phenomenon is illustrated in the two cylinder examples.

It is possible to modify the passive reflection event by imposing some voltage distribution over the free end. For an oscillating end voltage that is out-of-phase with the incoming wave, it is possible to extract electrical energy from it, i.e., energy harvesting. Examples of such an oscillating voltage with a particular radial distribution are given, that illustrate the amount of extracted energy as a function of the frequency of the incident monochromatic wave.

Keywords: Laminated piezoelectric circular cylinder; End reflection; End resonances; Energy harvesting

1. Introduction

We are concerned with the reflected field at the free end of a semi-infinite right laminated circular solid or hollow piezoelectric cylinder from a monochromatic wave source located afar. If the end cross-section and lateral surface(s) are traction-free and there is no other external energy exchange, the reflection is a passive event in which the outgoing field is made up of all available propagating waves and edge vibration modes.

* Corresponding author.
E-mail address: dong@seas.ucla.edu (S.B. Dong).

0020-7683/$ - see front matter
doi:10.1016/j.ijsolstr.2005.08.013

All of these modes in combination with the incoming wave satisfy the prescribed traction and electrical end conditions. But, if an oscillating voltage is applied to the free end, it is possible to control the form of the outgoing field. The extent to which the reflected wave field can be modified by an applied voltage on the end cross-section is intriguing. Herein, both passive and active phenomena are investigated for incoming monochromatic axisymmetric and flexural waves, i.e., for circumferential modes $m = 0$ and $m = 1$, respectively, in a Fourier representation of the θ-dependence. Linear three-dimensional piezoelectricity is used.

The reflected wave field is represented by propagating waves and edge vibration modes obtained from a free vibration analysis. Herein, this modal basis is established by a semi-analytical finite element analysis set forth by Siao et al. (1994). In Bai et al. (2004), a literature review was given of the various methods for extracting these vibration modes in a circular piezoelectric cylinder. The modal amplitudes of the reflected field can be determined by either a virtual work principle or a least-square minimization of boundary residuals. In Bai et al. (2004), they used such modal data to construct steady-state Green's functions.

As part of this study, end resonant modes are also sought. End resonance is manifested by large (but bounded) amplitude displacements at the end of the cylinder, and such a phenomenon occurs in a very narrow band-width typically below the first axisymmetric cutoff frequency ($m = 0$). End resonance in isotropic circular cylinders was first observed experimentally by Oliver (1957) and determined analytically by McNiven (1961) to within the 13% of Oliver's frequency observation using three modes of the reflected wave field spectrum. This result was further refined to within 0.5% by Zemanek (1972) with nine modes.

There is a sizeable literature on wave reflection studies of plates and cylinders. They are all based on a wave function expansion, where the modal amplitudes are determined by either some form of least-squares minimization or a variational principle. For planar and axisymmetric waves in homogeneous, isotropic plates and circular cylinders, see Torvik (1967), Wu and Plunkett (1972), Gregory and Gladwell (1983), Kim and Steele (1989). Karunasena et al. (1991) studied the reflection of planar waves at the free end of a laminated composite plate, and Rattanawangcharoenn et al. (1994) studied the corresponding problem of axisymmetric and flexural waves in a laminated composite circular cylinder. Taweel et al. (2000) explored the reflected wave field in a semi-infinitely long laminated composite cylinder with a general cross-section.

After summarizing the modal analysis method, passive end reflection is considered. Calculations for two piezoelectric cylinders due to incident axisymmetric and flexural waves are given as illustrations. End resonances in these two cylinders are shown. An application of a oscillating voltage at the free end is essentially a forced input. It is shown that if such a voltage is out-of-phase with the incident wave, energy can be extracted from this wave.

2. Preliminaries and summary of eigenproblems

For a semi-infinite laminated piezoelectric circular cylinder, adopt cylindrical coordinates (r, θ, z) with the origin located at the center in the end cross-section, see Fig. 1. The primary dependent variables are: mechanical displacement $\mathbf{u} = [u_r, u_\theta, u_z]$; stress $\mathbf{T} = [T_{rr}, T_{\theta\theta}, T_{zz}, T_{\theta z}, T_{rz}, T_{r\theta}]^{\mathrm{T}}$; strain $\mathbf{S} = [S_{rr}, S_{\theta\theta}, S_{zz}, S_{\theta z}, S_{zr}, S_{r\theta}]^{\mathrm{T}}$; electric displacement $\mathbf{D} = [D_r, D_\theta, D_z]^{\mathrm{T}}$; and electric field $\mathbf{E} = [E_r, E_\theta, E_z]^{\mathrm{T}}$, where $\mathbf{E} = -\nabla\phi$ with ϕ as the electric potential. These variables are inter-related by strain–displacement and constitutive relations, i.e., respectively,

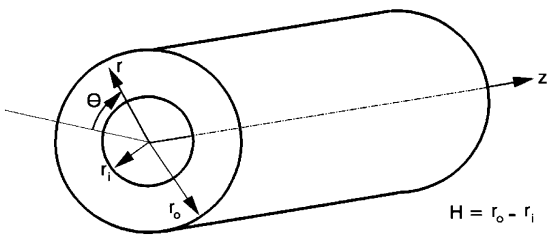

Fig. 1. Geometry of a hollow piezoelectric cylinder with r_i and r_o as inner and outer radii.

$$\mathbf{q} = \mathbf{L}\mathbf{v}, \tag{1}$$

$$\mathbf{Q} = \mathbf{C}^{*}\mathbf{q} \quad \text{with } \mathbf{C}^{*} = \begin{pmatrix} \mathbf{c} & -\mathbf{e}^{\mathbf{T}} \\ \mathbf{e} & \boldsymbol{\varepsilon} \end{pmatrix}, \tag{2}$$

where $\mathbf{c}$, $\mathbf{e}$ and $\boldsymbol{\varepsilon}$ are matrices of elastic anisotropic moduli (6×6), piezoelectric constants (3×6) and permittivities (3×3), respectively, and $\mathbf{q}$, $\mathbf{Q}$ and $\mathbf{v}$ are the combined electro-mechanical dependent variables.

$$\mathbf{q} = \begin{Bmatrix} \mathbf{S} \\ \mathbf{E} \end{Bmatrix}_{9\times1}, \qquad \mathbf{Q} = \begin{Bmatrix} \mathbf{T} \\ \mathbf{D} \end{Bmatrix}_{9\times1}, \qquad \mathbf{v} = \begin{Bmatrix} \mathbf{u} \\ \phi \end{Bmatrix}_{4\times1}. \tag{3}$$

There are as many sets of $\mathbf{c}$, $\mathbf{e}$, $\boldsymbol{\varepsilon}$ as the number of distinct layers in the cylinder.

Non-dimensionalization is used to circumvent numerical anomalies due to large differences between the material data quoted in their usual units. In explanation of the non-dimensionalization, regard all quantities on the right-hand and left-hand sides of the equations, respectively, as the dimensional and corresponding dimensionless forms. Four key parameters are needed: (1) total cylinder thickness H, (2) an elastic modulus c^0, (3) a piezoelectric constant e^0, and (4) mass density ρ^0, where these properties are selected from a particular laminate in the cylinder. Reference dielectric constant ε^0 and electric field E^0 can then be defined as $\varepsilon^0 = (e^0)^2/c^0$ and $E^0 = c^0/e^0$. The independent and dependent variables and material properties, respectively, are then normalized as

$$\begin{aligned}
&r = \frac{r}{H}, \quad z = \frac{z}{H} \quad (i = r,\theta,z), \quad t = \frac{t}{H}\sqrt{\frac{c^0}{\rho^0}}, \\
&u_i = \frac{u_i}{H} \quad (i = r,\theta,z), \quad T_p = \frac{T_p}{c^0}, \quad S_p = S_p \quad (p = 1,2,\ldots,6), \\
&D_k = \frac{D_k}{e^0}, \quad E_k = \frac{E_k}{E^0} \quad (k = 1,2,3), \\
&c_{pq} = \frac{c_{pq}}{c^0}, \quad \varepsilon_{ij} = \frac{\varepsilon_{ij}}{\varepsilon^0}, \quad e_{ip} = \frac{e_{ip}}{e^0}, \quad \rho_i = \frac{\rho_i}{\rho^0} \quad (p,q = 1,2,3,\ldots,6).
\end{aligned} \tag{4}$$

Lastly, the normalized charge ρ_e and body force density component f_i are given by

$$\rho_e = \frac{H\rho_e}{e^0}, \quad f_i = \frac{Hf_i}{c^0} \quad (i = r,\theta,z). \tag{5}$$

This non-dimensionalization enables all dimensionless variables and equations to have the same forms as their dimensional counterparts.

In Siao et al.'s (1994) semi-analytical finite element formulation, discretization of the laminated cylinder occurs in the thickness direction with three-node cylindrical laminas, each capable of having its own piezoelectric properties and thickness. Radial quadratic interpolations are used in each element, with the axial, circumferential and time dependencies left undetermined at the outset. The discrete equations of motion for free vibration are

$$\mathbf{K}_1\mathbf{V} + \mathbf{K}_2\mathbf{V}_{,\theta} + \mathbf{K}_3\mathbf{V}_{,z} - \mathbf{K}_4\mathbf{V}_{,\theta\theta} - \mathbf{K}_5\mathbf{V}_{,\theta z} - \mathbf{K}_6\mathbf{V}_{,zz} + \mathbf{M}\ddot{\mathbf{V}} = \mathbf{0}, \tag{6}$$

where $\mathbf{V} = \mathbf{V}(\theta, z, t)$ is the nodal variables array of the finite element model. Stiffness matrices $\mathbf{K}_1$, $\mathbf{K}_4$, $\mathbf{K}_5$, $\mathbf{K}_6$ and consistent mass matrix $\mathbf{M}$ are symmetric, while stiffness matrices $\mathbf{K}_2$ and $\mathbf{K}_3$ are antisymmetric; their forms can be found in Siao et al. (1994). Traction-free lateral surfaces in the hollow cylinder are assumed, i.e., $T_{rr} = T_{r\theta} = T_{rz} = 0$. Surface electrical condition may take the form of an opened circuit (surface is uncoated) where the radial electric displacement component, $D_r = 0$, or a short-circuited condition (a coated lateral surface that is grounded) where the voltage $\phi = 0$.

For free vibrations, the solution form is

$$\mathbf{V} = \mathbf{V}_m \exp\{\mathrm{i}(k_m z + m\theta - \omega t)\}, \tag{7}$$

where ω is the circular frequency, (k_m, m) are the axial and circumferential wave numbers, and array $\mathbf{V}_m$ represents the nodal amplitudes of the finite element model. Mode number m is assigned an integer value to assure circumferential periodicity. Substitution of Eq. (7) into Eq. (6) and factoring out the exponential term give

$$\left(\mathbf{K}_1 + \mathrm{i}m\mathbf{K}_2 + \mathrm{i}k_m\mathbf{K}_3 + m^2\mathbf{K}_4 + mk_m\mathbf{K}_5 + k_m^2\mathbf{K}_6\right)\mathbf{V}_m - \omega^2\mathbf{M}\mathbf{V}_m = 0, \tag{8}$$

where either ω^2 or k_m can act as the eigenvalue, thus giving the following two eigenproblems.

2.1. Real wave numbers

With k_m assigned and ω^2 as the eigenvalue, Eq. (8) becomes

$$\left[(\mathbf{K}_1 + m^2\mathbf{K}_4 + mk_m\mathbf{K}_5 + k_m^2\mathbf{K}_6) + \mathrm{i}(m\mathbf{K}_2 + k_m\mathbf{K}_3)\right]\mathbf{V}_m = \omega^2\mathbf{M}\mathbf{V}_m. \tag{9}$$

The left-hand side matrix is Hermitian, so only real ω^2's are admitted. This eigenproblem enables the spectra of all propagating modes to be established.

2.2. Complex wave numbers

By assigning ω^2, Eq. (8) takes on the form of a second order algebraic eigenproblem in k_m.

$$\left[(\mathbf{K}_1 + m^2\mathbf{K}_4 - \omega^2\mathbf{M} + \mathrm{i}m\mathbf{K}_2) + k_m(m\mathbf{K}_5 + \mathrm{i}\mathbf{K}_3) + k_m^2\mathbf{K}_6\right]V_m = 0. \tag{10}$$

The eigenpairs of Eq. (10) are the wave number k_{mn} and associated right-modal matrix $\mathbf{\Phi}_{mn}$. The adjoint problem yields the same wave numbers k_{mn} and the left-handed modal matrix $\mathbf{\Psi}_{mn}$. Real wave numbers k_{mn} represent propagating waves, while the complex conjugate pairs describe standing vibrations with spatially decaying amplitudes. The corresponding stress eigenvectors are evaluated by Eqs. (1) and (2). These eigendata provide the modal basis for representation of the reflected field.

3. End reflection

Consider the passive reflection of an incoming monochromatic wave $\mathbf{V}_m^{\mathrm{in}}(\theta, z, t)$ traveling in a negative z-direction, i.e.,

$$\mathbf{V}_m^{\mathrm{in}}(\theta, z, t) = a^{\mathrm{in}}\boldsymbol{\phi}_{mp}\mathrm{e}^{\mathrm{i}(-k_{mp}z + m\theta - \omega t)}, \quad z \geqslant 0, \tag{11}$$

where superscript in denotes an incident wave and a^{in}, (k_{mp}, m), and ω are the amplitude, wave numbers, and frequency of the p-th propagating mode. When this wave impinges upon the end $z = 0$, a reflected wave field $\mathbf{V}_m^{\mathrm{rf}}$ is generated (designated by superscript *rf*), which can be approximated by a modal sum of right eigenvectors

$$\mathbf{V}_m^{\mathrm{rf}}(\theta, z, t) = \sum_{n=1}^{N} a_{mn}\boldsymbol{\phi}_{mn}\mathrm{e}^{\mathrm{i}(k_{mn}z + m\theta - \omega t)}, \quad z \geqslant 0, \tag{12}$$

where a_{mn}'s are amplitudes to be determined. For simplicity, suppress the exponential factor involving θ and ω and their associated subscript m in the wave forms; no confusion should arise. Recasting Eqs. (11) and (12) in the abbreviated forms yields

$$\mathbf{V}^{\mathrm{in}}(z) = \quad a^{\mathrm{in}}\boldsymbol{\phi}_p\mathrm{e}^{-\mathrm{i}k_p z}, \quad \mathbf{V}^{\mathrm{rf}}(z) = \sum_{n=1}^{N} a_n\boldsymbol{\phi}_n\mathrm{e}^{\mathrm{i}k_n z}, \quad z \geqslant 0. \tag{11a, 12a}$$

Observe that wave numbers with negative imaginary parts are excluded in representation (12) as they are unbounded in the domain occupied by the semi-infinite cylinder.

In passive reflection, the end at $z = 0$ is traction-free.

$$T_{zz} = T_{z\theta} = T_{zr} = 0, \quad z = 0. \tag{13}$$

Electrically, either a voltage ϕ (grounded) or electric displacement D_z (open circuit) can be prescribed to vanish at the end

$$\phi = 0 \quad \text{or} \quad D_z = 0, \quad z = 0. \tag{14}$$

Both electrical conditions will be considered. Traction-free end and electrical conditions will be enforced at each Gaussian integration point in all elements comprising the cylinder's thickness profile. To this end, introduce the ordered arrays $\mathbf{t}_n$, $\mathbf{p}_n$, $\mathbf{d}_n$ and $\mathbf{u}_n$

$$\begin{aligned}
\mathbf{t}_n &= [T_{zz,1-1,n}, T_{z\theta,1-1,n}, T_{zr,1-1,n}, T_{zz,1-2,n}, \ldots, T_{zz,\mathrm{NE}-3,n}, T_{z\theta,\mathrm{NE}-3,n}, T_{zr,\mathrm{NE}-3,n}]^{\mathrm{T}},\\
\mathbf{p}_n &= [\phi_{1-1,n}, \phi_{1-2,n}, \phi_{1-3,n}, \phi_{2-1,n}, \ldots, \phi_{\mathrm{NE}-2,n}, \phi_{\mathrm{NE}-3,n}]^{\mathrm{T}},\\
\mathbf{d}_n &= [D_{z,1-1,n}, D_{z,1-2,n}, D_{z,1-3,n}, D_{z,2-1,n}, \ldots, D_{z,\mathrm{NE}-2,n}, D_{z,\mathrm{NE}-3,n},]^{\mathrm{T}},\\
\mathbf{u}_n &= [u_{r,1-1,n}, u_{\theta,1-1,n}, u_{z,1-1,n}, u_{r,1-2,n}, \ldots, u_{r,\mathrm{NE}-3,n}, u_{\theta,\mathrm{NE}-,n}, u_{z,\mathrm{NE}-3,n}]^{\mathrm{T}}.
\end{aligned} \tag{15}$$

The ordered subscripts are defined as follows: (1) the first denotes the traction and electrical displacement component, except for $\boldsymbol{\phi}$ which is a scalar, (2) the second gives the element number followed by a dash and the Guassian point within the element, and (3) the last identifies the nth mode in the spectra; and NE stands for the total number of elements. Thus, the incident and reflected fields at $z = 0$ can be written as

$$\begin{aligned}
&\mathbf{f}^{\mathrm{in}} = a^{\mathrm{in}}\mathbf{f} \quad \text{and} \quad \mathbf{f}^{\mathrm{rf}} = \mathbf{F}\mathbf{a},\\
&\mathbf{g}^{\mathrm{in}} = a^{\mathrm{in}}\mathbf{g} \quad \text{and} \quad \mathbf{g}^{\mathrm{rf}} = \mathbf{G}\mathbf{a}
\end{aligned} \tag{16}$$

where

$$\begin{aligned}
&\mathbf{a} = [a_1, a_2, \ldots, a_n, \ldots, a_N]^{\mathrm{T}},\\
&\mathbf{f} = \begin{Bmatrix} \mathbf{t}^{\mathrm{in}} \\ \lambda^{\mathrm{in}} \end{Bmatrix}; \qquad \mathbf{F} = \begin{bmatrix} \mathbf{t}_1 & \mathbf{t}_2 & \cdots & \mathbf{t}_N \\ \lambda_1 & \lambda_2 & \cdots & \lambda_N \end{bmatrix},\\
&\mathbf{g} = \begin{Bmatrix} \mathbf{u}^{\mathrm{in}} \\ \bar{\lambda}^{\mathrm{in}} \end{Bmatrix}; \qquad \mathbf{G} = \begin{bmatrix} \mathbf{u}_1 & \mathbf{u}_2 & \cdots & \mathbf{u}_N \\ \bar{\lambda}_1 & \bar{\lambda}_2 & \cdots & \bar{\lambda}_N \end{bmatrix}.
\end{aligned} \tag{17}$$

with λ_i and $\bar{\lambda}_i$ as conjugate electrical variables so that $\lambda_i = \mathbf{p}_i$ and $\bar{\lambda}_i = \mathbf{d}_i$ or vice versa, depending on the electrical end conditions.

Traction-free end (13) and electrical (14) conditions by means of Eqs. (16) and (17) take the form

$$\mathbf{f}^{\mathrm{in}} + \mathbf{f}^{\mathrm{rf}} \equiv a^{\mathrm{in}}\mathbf{f} + \mathbf{F}\mathbf{a} = 0. \tag{18}$$

Since a truncated set of modes is used, this enforcement at the Gaussian integration points will not be exact, so that a residual will remain, which is denoted by array ε

$$a^{\mathrm{in}}\mathbf{f} + \mathbf{F}\mathbf{a} = \varepsilon. \tag{19}$$

Least-square minimization or virtual work can be used to determine the reflection amplitudes $a_n's$ of this overdetermined system. The least-square solution for the a_n's is given by

$$\mathbf{a} = -a^{\mathrm{in}}[\langle \mathbf{F}, \mathbf{F}\rangle]^{-1}\{\langle \mathbf{F}, \mathbf{f}\rangle\} \equiv -a^{\mathrm{in}}\mathbf{g}^{\mathrm{in}}_{ls}, \tag{20}$$

where the bracket denotes the inner product

$$\langle \boldsymbol{\alpha}, \boldsymbol{\beta}\rangle \equiv \int_{r_{\mathrm{i}}}^{r_{\mathrm{o}}} \boldsymbol{\alpha}^{\mathrm{H}}\boldsymbol{\beta} r \, \mathrm{d}r. \tag{21}$$

Superscript H signifies complex conjugate transposition and r_{i} and r_{o} represent the inner and outer radius of the cylinder, respectively. Note that $\mathbf{F}^{\mathrm{H}}\mathbf{F}$ is Hermitian, and the values in $\mathbf{a}$ will occur as real and complex conjugate pairs. Solution by means of a virtual work principle (see Wu and Plunkett, 1972) asserts that the product of the conjugate variables vanish.

$$\boldsymbol{\delta}\langle \mathbf{G}, a^{\mathrm{in}}\mathbf{f} + \mathbf{F}\mathbf{a}\rangle = 0. \tag{22}$$

This method gives the reflected amplitudes **a** as

$$\mathbf{a} = -a^{\text{in}}[\langle \mathbf{G}, \mathbf{F} \rangle]^{-1}\{\langle \mathbf{G}, \mathbf{f} \rangle\} \equiv -a^{\text{in}}\mathbf{g}^{\text{in}}_{vw}. \tag{23}$$

Here, conjugate electrical variables are used in **G**, **f** and **F** Once the amplitudes are established, they may be normalized with that of the incident wave, i.e., $a_n = a_n/a^{\text{in}}$, $n = 1, 2, \ldots, N$.

4. Energy flux

Passive reflection conserves energy. Since energy is only carried by the propagating modes, all participating outgoing propagating modes must collectively return the energy of the incident wave. An energy balance, expressed in terms of energy flux, i.e., the time-averaged value of the energy, can be used to measure the solution accuracy. The time-average value of the energy flux associated with the nth reflected propagating mode is given by

$$\mathscr{E}_n = |a_n|^2 \omega \,\text{Im}\langle \bar{\mathbf{t}}_n, \bar{\mathbf{u}}_n \rangle + \langle \bar{\mathbf{d}}_n, \bar{\mathbf{p}}_n \rangle \equiv |a_n|^2 J_n, \tag{24}$$

where the overbars denote complex conjugation. The total energy of the outgoing field is the sum of all N_{pr} propagating modes.

$$\mathscr{E}_{\text{out}} = \sum_{n=1}^{N_{\text{pr}}} \mathscr{E}_n. \tag{25}$$

The energy flux of the incident field is given by

$$\mathscr{E}_{\text{in}} = \omega \,\text{Im}\left\{ \langle \bar{\mathbf{t}}^{\text{in}}, \bar{\mathbf{u}}^{\text{in}} \rangle + \langle \bar{\mathbf{d}}^{\text{in}}, \bar{\mathbf{p}}^{\text{in}} \rangle \right\}. \tag{26}$$

The proportion of energy carried by the nth reflected propagating wave is $\mathscr{E}_n/\mathscr{E}_{\text{in}}$. A useful index to measure the solution accuracy is the percentage error in energy balance δ defined by

$$\delta = \left[1 - \sum_{n=1}^{N_{\text{pr}}} \frac{\mathscr{E}_n}{\mathscr{E}_{\text{in}}} \right] \times 100. \tag{27}$$

A serious departure of δ from zero indicates an error in energy balance.

5. Passive end reflection examples

Two examples are presented to illustrate passive reflection in piezoelectric bodies. In these examples, two hollow cylinders (inside and outside radii of $r_{\text{in}} = 0.5$m and $r_{\text{out}} = 1.5$m) are considered, both with open-circuit electrical conditions on their lateral surfaces. Both are composed of a PZT-4 material whose properties are given in Berlincourt et al. (1964). One cylinder is homogeneous with its crystallographic axes aligned in the coordinate directions. The second cylinder is composed of two equal thickness layers whose longitudinal crystallographic axes are at $\pm 30^0$ with the generator. The properties for these two cases are

Homogeneous cylinder

$$\mathbf{c} = \begin{bmatrix} 5.42969 & 3.03906 & 2.90234 & \cdot & \cdot & \cdot \\ \cdot & 5.42969 & 2.90234 & \cdot & \cdot & \cdot \\ \cdot & \cdot & 4.49219 & \cdot & \cdot & \cdot \\ \cdot & \cdot & \cdot & 1.0 & \cdot & \cdot \\ \cdot & \text{symmetric} & \cdot & \cdot & 1.0 & \cdot \\ \cdot & \cdot & \cdot & \cdot & \cdot & 1.19531 \end{bmatrix}_{0^0},$$

$$\mathbf{e} = \begin{bmatrix} \cdot & \cdot & \cdot & \cdot & 0.84106 & \cdot \\ \cdot & \cdot & \cdot & 0.84106 & \cdot & \cdot \\ -0.34437 & -0.34437 & 1.0 & \cdot & \cdot & \cdot \end{bmatrix}_{0^0},$$

$$\boldsymbol{\varepsilon} = \begin{bmatrix} 1.46632 & \cdot & \cdot \\ \cdot & 1.46632 & \cdot \\ \cdot & \cdot & 1.29229 \end{bmatrix}_{0^0}. \tag{28}$$

Two-layer cylinder

$$\mathbf{c} = \begin{bmatrix} 5.42969 & 3.00488 & 2.93652 & \mp 0.05920 & \cdot & \cdot \\ \cdot & 5.17334 & 2.92432 & \mp 0.21566 & \cdot & \cdot \\ \cdot & \cdot & 4.70459 & \mp 0.19029 & \cdot & \cdot \\ \cdot & \cdot & \cdot & 1.02197 & \cdot & \cdot \\ \cdot & \text{symmetric} & \cdot & \cdot & 1.04883 & \mp 0.08457 \\ \cdot & \cdot & \cdot & \cdot & \cdot & 1.14648 \end{bmatrix}_{\pm 30^0},$$

$$\mathbf{e} = \begin{bmatrix} & & & & 0.72838 & \pm 0.42053 \\ \mp 0.17219 & \pm 0.62666 & \mp 0.29884 & 0.65525 & \cdot & \cdot \\ -0.29823 & -0.37136 & 0.93915 & \pm 0.29387 & \cdot & \cdot \end{bmatrix}_{0^0}, \tag{29}$$

$$\boldsymbol{\varepsilon} = \begin{bmatrix} 1.46632 & \cdot & \cdot \\ \cdot & 1.42280 & \mp 0.07535 \\ \cdot & \cdot & 1.33581 \end{bmatrix}_{0^0}.$$

The four reference parameters are (1) $H = 1$ m, (2) $c^0 = c_{44} = 25.6$ GPA, (3) $e^0 = e_{33} = 15.1$ C/m^2 and (4) $\rho^0 = 7.50 \times 10^4$ kg/m^3 so that $\varepsilon^0 = 8.90664 \times 10^{-9}$ F/m and $E^0 = 1.69536 \times 10^9$ N/C. Based on these values, the normalized frequency is given by

$$\omega = \frac{\omega}{\omega_0} \quad \text{where } \omega_0 = \frac{1}{H}\sqrt{c^0/\rho^0} = 584.24 \text{ rad/s}. \tag{30}$$

Solution accuracy obviously depends on finite element discretization. Drawing from the authors' previous numerical modeling experience (see Bai et al., 2004), and verified by additional convergence studies (not shown here), a 20 element model (808 dof's) over the frequency range of consideration ($1.5 \leqslant \omega \leqslant 4.5$) was deemed to an adequate model.

Example 1. For the homogeneous PZT-4 hollow cylinder, the end at $z = 0$ is traction-free with open-circuit electrical condition. Consider the reflection of the first incoming propagating mode for circumferential wave numbers $m = 0$ and $m = 1$. The propagation spectra for these two circumferential modes in the frequency range are shown in Fig. 2. Note that for $m = 0$, there are torsional modes which are shown by dotted spectral lines. They do not participate in the reflection of the lowest incoming extensional wave.

For $m = 0$, there are two extensional cutoff frequencies $\omega = 2.225$, 3.983 for $k_0 = 0$ and another of $\omega = 2.205$ at the minimum point of the second branch, see Fig. 2 Wave numbers k_0 to the left of $\omega = 2.205$ refer to "backward waves," or waves with a negative group velocity. In Fig. 3(a,b) and (c,d) are shown, respectively, the normalized amplitudes and the proportion of energy in each reflected mode in our frequency range of interest. For incoming wave frequencies below $\omega = 2.205$, only one propagating mode is reflected. In the frequency range ($2.205 \leqslant \omega \leqslant 2.225$), three propagating modes share in the return of the incoming energy.[1] This energy partition can be seen in Fig. 3d where I_1 decreases, I_2 increases, and I_3 first increases then decreases with increasing incident wave frequency. With incoming wave frequencies above $\omega = 2.225$, only

[1] In this range, the mirror image of the propagating backward wave about the frequency axis must be used in the reflected wave field. This wave possesses a positive group velocity.

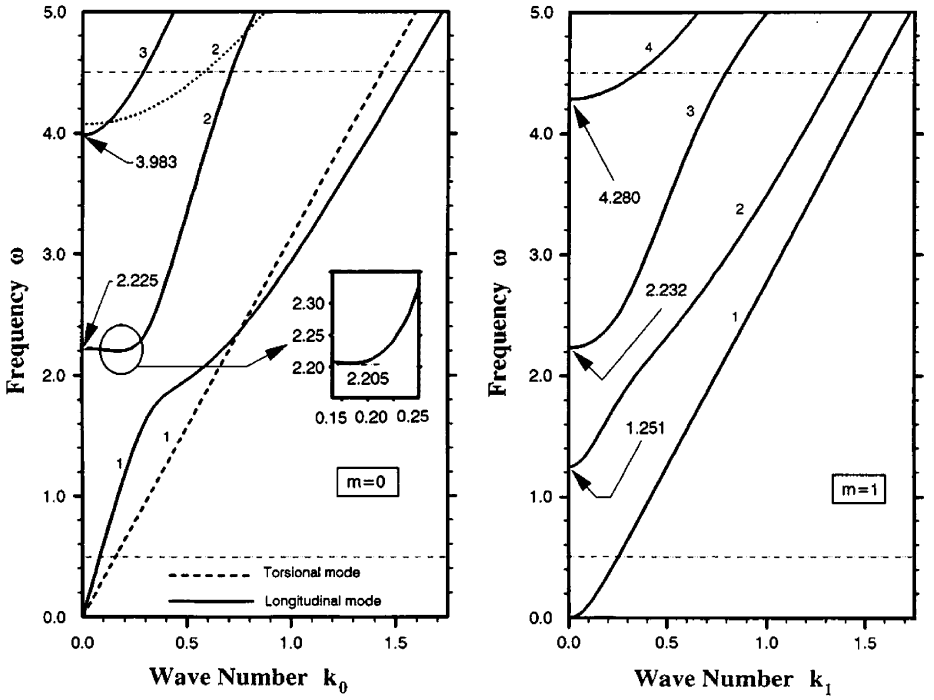

Fig. 2. Frequency spectra for homogeneous cylinder.

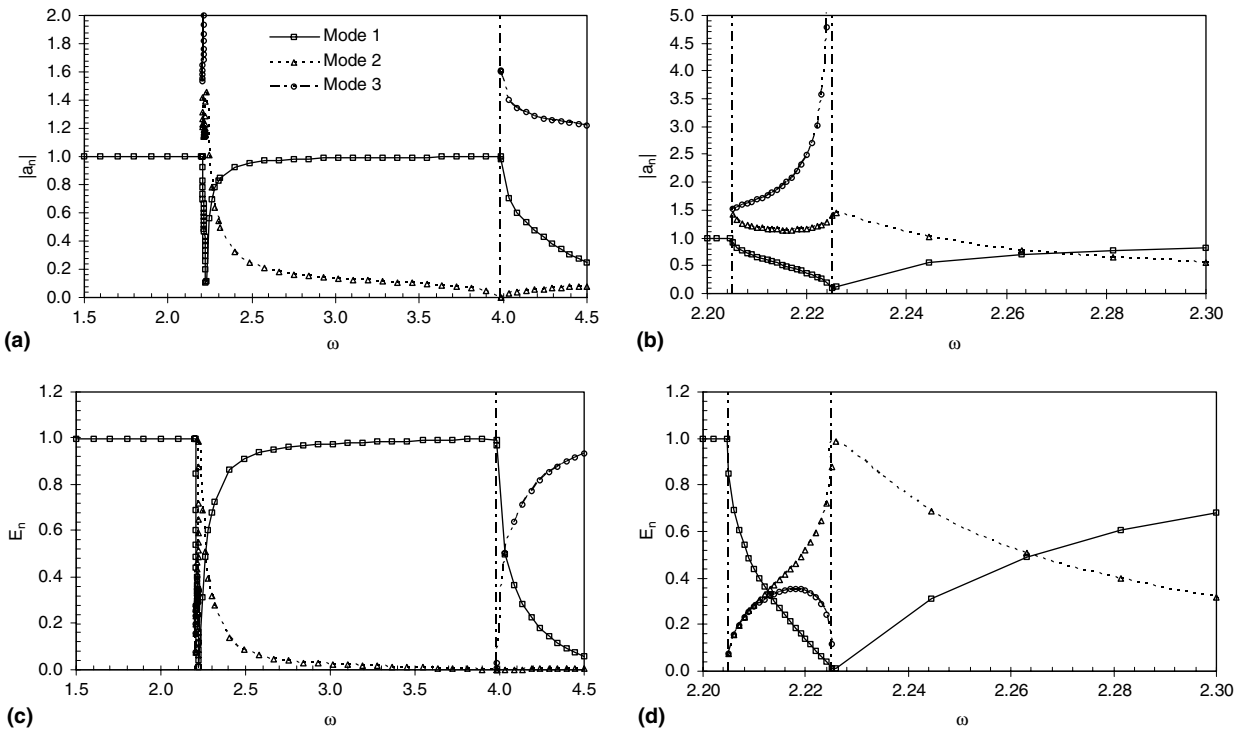

Fig. 3. Reflection in homogeneous PZT4 cylinder with incident mode (0, 1).

two propagating modes are available. At the outset in this frequency interval, the second mode carries the bulk of the energy, but shortly thereafter (at roughly $\omega = 2.26$), the first mode dominates. As the incoming wave frequency increases beyond $\omega = 3.983$, another propagating mode is cut on. In this frequency range, mode 1 carries the majority of return energy initially, but cedes this role to mode 3 as the frequency increases. The second mode is not a factor throughout this frequency interval.

For $m = 1$, similar plots of normalized amplitudes and proportion of energy of each reflected mode are shown in Fig. 4(a) and (b) for an incoming flexural incident wave. The lowest three cutoff frequencies are $\omega = 1.251$, 2.232, and 4.280 as shown in Fig. 2. There are no waves with negative group velocity for $m = 1$. Hence, all reflected wave fields over a given frequency interval before encountering the next higher cutoff frequency is composed of the available propagating waves, i.e., below cutoff frequency $\omega = 1.251$, only one propagating wave is reflected; between $1.251 \leqslant \omega \leqslant 2.232$, two propagating waves are possible; etc. Fig. 4 shows the energy partitioning of the incoming energy in the outgoing propagating modes.

Since both least-squares and virtual work methods were used for the amplitudes of the reflected field, a comparison of the percentage energy errors between them was made for $m = 0$. The results in Table 1 show both methods converging with increasing modes, but virtual work is decidedly more efficient. However, if the criterion is based on satisfying traction-free and open electrical conditions at the Gaussian points over the entire end cross-section, substantially more terms are needed beyond that for energy convergence. In this case, the least-squares method is usually more effective.

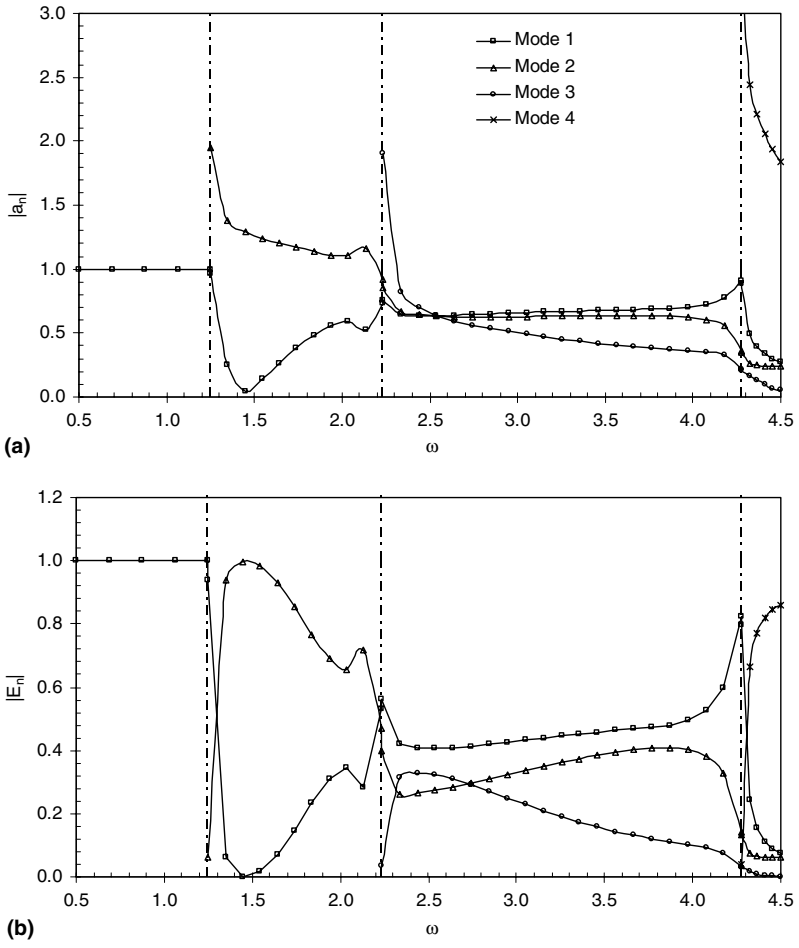

Fig. 4. Reflection in homogeneous PZT4 cylinder with incident mode (1, 1).

Table 1
Comparison results between two proposed methods

No. of modes	Percentage energy error	
	Variational method	Least-square method
9	0.0120762953	1.5945280822
18	0.0123930158	0.1093008450
38	0.0010000136	0.0137479347
122	0.0000153697	0.0000153697

Twenty elements are used in the computation.

Example 2. For the two-layer cylinder, the same end conditions used in Example 1 were adopted, i.e., a surface which is traction-free with open-circuit electrical condition. Consider the reflection of the lowest incoming propagating mode for circumferential wave numbers $m = 0, 1$. The spectral plots are shown in Fig. 5, where the cutoff frequencies are indicated. Unlike Example 1, there are no pure extensional nor pure torsional modes for $m = 0$ as these behaviors are coupled in the lowest two modes.

Fig. 6(a,b) and (c,d) show the normalized amplitudes and proportions of energy of each reflected mode for $m = 0$. Backward waves for wave numbers k_0 to the left of cutoff frequency $\omega = 2.145$ are again evident. For incident waves of frequency $\omega < 2.145$, two propagating modes are possible in the reflected field where the extensional mode is predominant, i.e., the lowest one of the two modes. In the narrow range $2.145 \leqslant \omega \leqslant 2.163$, four propagating modes can occur in the reflected field, where the extensional (first) mode predominates. For $\omega > 2.163$, three propagating modes occur where the lowest mode again carries the most energy. At frequencies $\omega > 3.864$, only the first and fourth modes are active, with the first mode initially carrying most of the energy but relinquishing this role to mode 4 as the frequency increases.

Fig. 7(a) and (b) show normalized amplitudes and proportions of energy of each of the reflected modes for $m = 1$. The over all behavior for this circumferential mode is similar to that of the homogeneous PZT-4 cylinder.

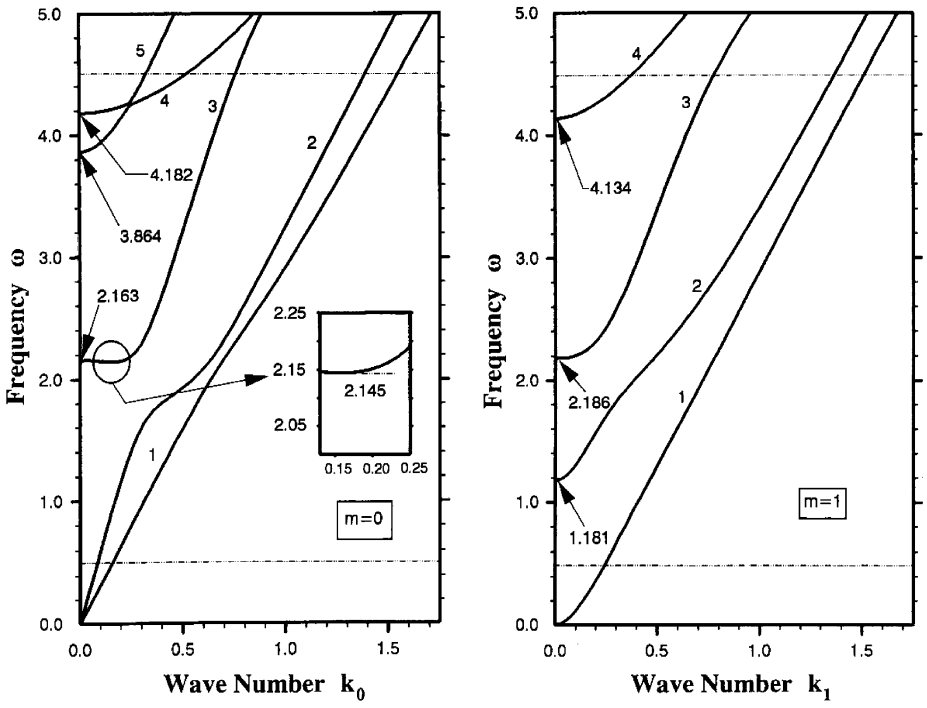

Fig. 5. Frequency spectra for two-layer PZT4 cylinder.

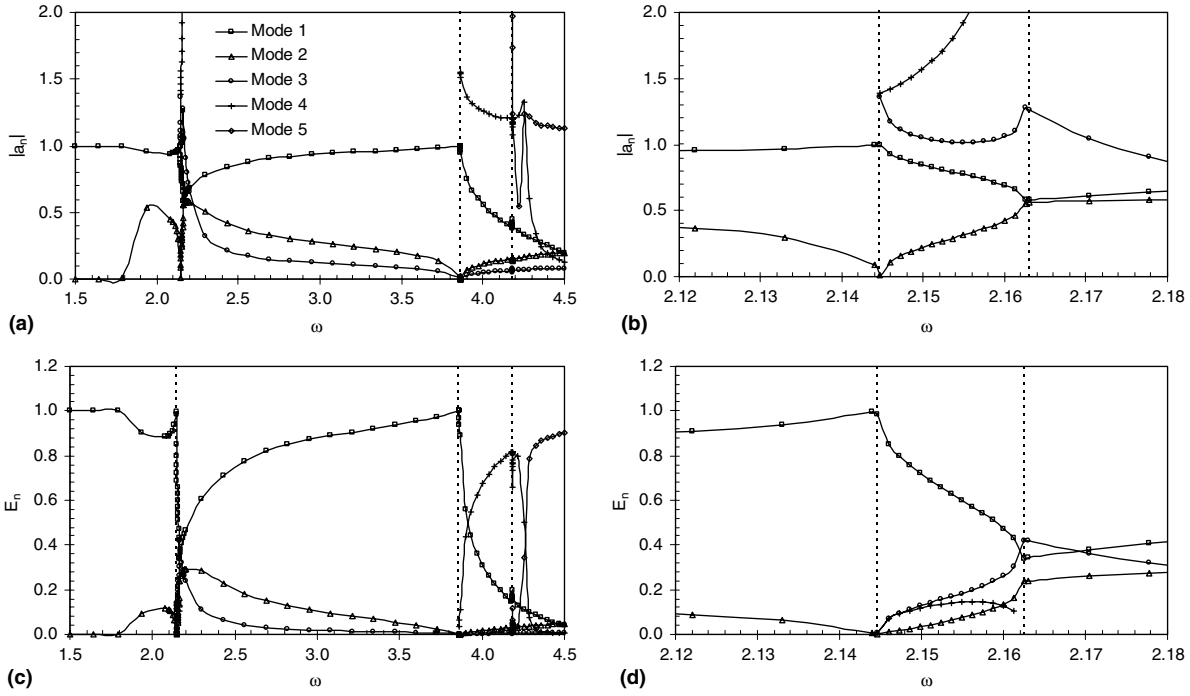

Fig. 6. Reflection in two-layer PZT4 cylinder with incident mode (0, 1).

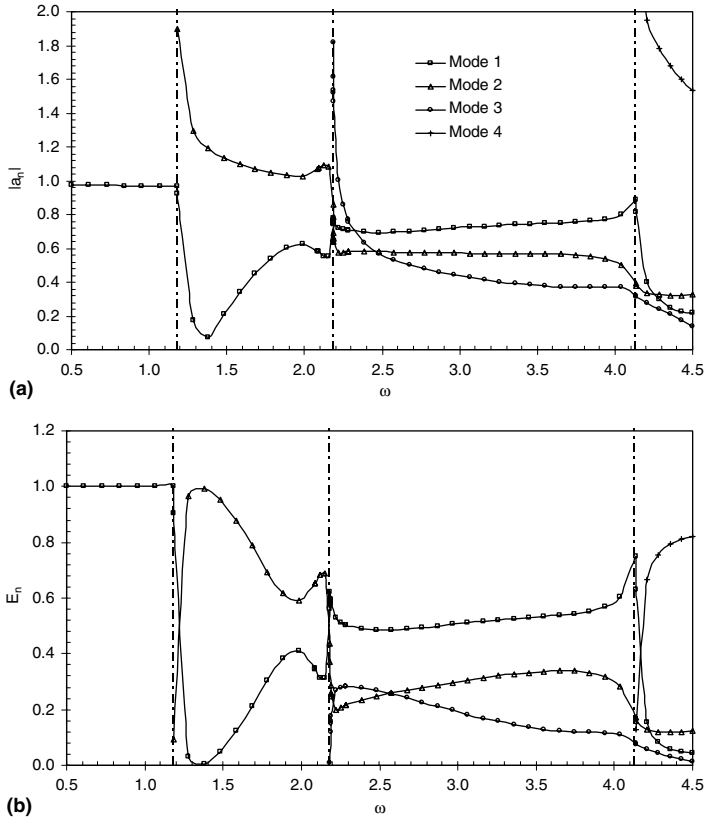

Fig. 7. Reflection in two-layer PZT4 cylinder with incident mode (1, 1).

6. End resonance

End resonances due to incident axisymmetric waves, i.e., $m = 0$, were observed in both cylinders. These resonances, as manifested by large end displacements, occurred at $\omega = 1.9425$ and $\omega = 1.8826$, respectively, for the homogeneous and two-layer cylinders. Both of these frequencies are just below their respective first cutoff frequencies. Fig. 8 shows displacements and voltage distributions for the homogeneous cylinder at frequencies (1) just below, (2) at resonance and (3) just above, i.e., at $\omega = [1.92, 1.9425, 2.00]$, respectively. The voltage dis-

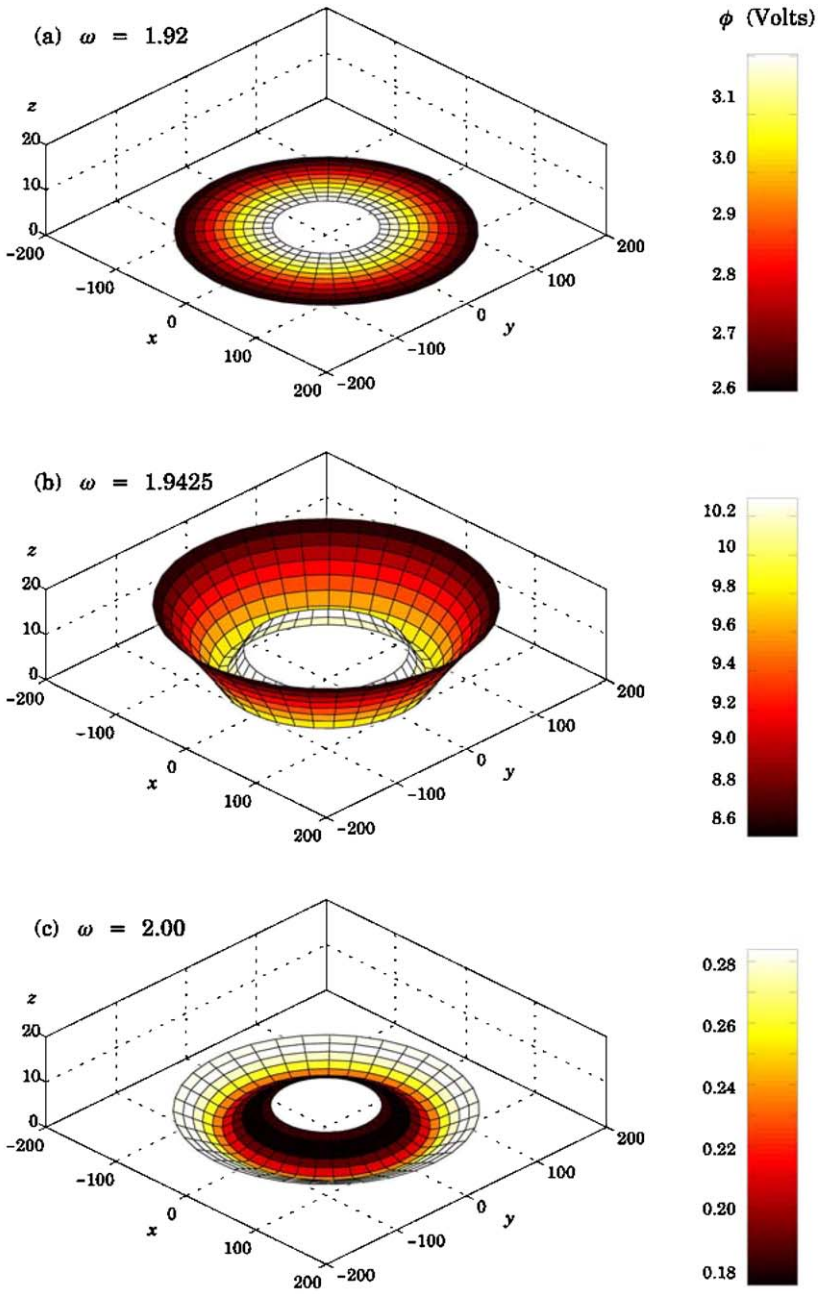

Fig. 8. End resonance in homogeneous PZT4 cylinder.

tribution appears in a colored scale. The large amplitude displacements and high voltage at the resonant requency can be seen. Also, shown are these patterns slightly below and above the resonant frequency, so that the dramatic changes can be observed. Similarly, Fig. 9 shows the data for the two-layer cylinder, where displacement and voltage plots are given at three frequencies, i.e., $\omega = [1.86, 1.8826, 1.91]$, respectively. The same phenomenon of large and dramatic increases in displacements and voltage is seen. Careful searches were conducted for the end resonances in these two cylinders for $m = 1$, but none were found in the frequency range considered.

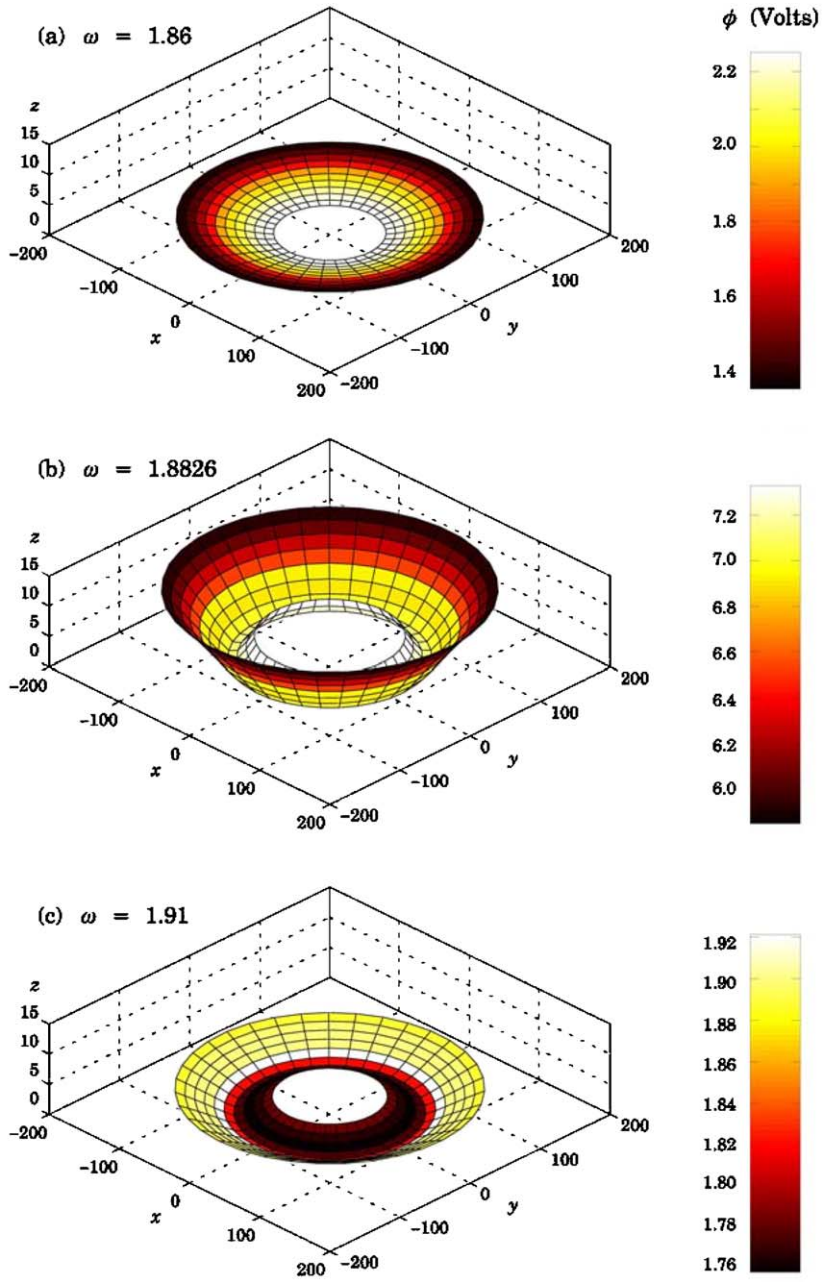

Fig. 9. End resonance in two-layer PZT4 cylinder.

7. Oscillating end voltage

An oscillating voltage applied at $z = 0$ generates time harmonic outgoing waves in a semi-infinite cylinder. In the absence of an incoming wave, the cylinder is essentially driven by this voltage, and the outgoing field can be represented by a modal sum of right eigenvectors. Consider an axisymmetric end voltage of amplitude ϕ_0 and frequency ω with a radial distribution given by $v(r)$. This end condition on a traction-free surface has the form

$$T_{zz} = T_{rz} = T_{\theta z} = 0, \quad \phi(r,t) = \phi_0 v(r) \mathrm{e}^{-\mathrm{i}\omega t}, \quad z = 0. \tag{31a}$$

By the notation of Eq. (17), this end condition is written as

$$\mathbf{f}^{\phi} = \phi_0 \boldsymbol{\mu} \quad \text{where } \boldsymbol{\mu} = \begin{Bmatrix} \mathbf{0} \\ v \end{Bmatrix}, \tag{31b}$$

where $v = v(r)$ contains the nodal distribution of voltages. The outgoing field in terms of modal sum of right eigenvectors at $z = 0$ is given by

$$\mathbf{R}_s^{\phi} = \mathbf{F}_s \mathbf{b}. \tag{32}$$

The complex amplitudes in $\mathbf{b}$ are determined by equating Eq. (32) to Eq. (31b).

$$\begin{Bmatrix} \mathbf{0} \\ v \end{Bmatrix} = \mathbf{F}_s \mathbf{b}. \tag{33}$$

The least-squares solution of Eq. (33) is

$$\mathbf{b} = \phi_0 [\langle \mathbf{F}, \mathbf{F} \rangle]^{-1} [\langle \mathbf{F}, \boldsymbol{\mu} \rangle] \equiv \phi_0 \mathbf{g}^{\phi}. \tag{34}$$

Now, consider the presence of an incoming monochromatic wave whose reflection occurs with an oscillating end voltage. This oscillating voltage will obviously alter the reflected field. The end condition for this case is given by Eq. (31). A worthy objective would be to determine the magnitude ϕ_0 of the given distribution $v(r)$ that minimizes the energy flux carried by the outgoing propagating waves. This problem is one of passive vibration control. Since both passive end reflection and forced vibration by an electric potential are linear, the reflected field is the sum of these processes, i.e., the sum of Eqs. (23) and (34)

$$\mathbf{a} = -a^{\mathrm{in}} [\langle \mathbf{G}, \mathbf{F} \rangle]^{-1} \{ \langle \mathbf{G}, \mathbf{f} \rangle \} + \phi_0 [\langle \mathbf{F}, \mathbf{F} \rangle]^{-1} [\langle \mathbf{F}, \boldsymbol{\mu} \rangle] \equiv -a^{\mathrm{in}} \mathbf{g}^{\mathrm{in}} + \phi_0 \mathbf{g}^{\phi}. \tag{35}$$

The difference in signs between a^{in} and ϕ_0 indicates a π radians phase difference between these two sources, i.e. $-1 = \mathrm{e}^{\mathrm{i}\pi}$. If ϕ_0 is found to be positive, the end voltage is out-of-phase with the incident wave. The components of $\mathbf{a}$ are

$$a_n = -g_n^{\mathrm{in}} a^{\mathrm{in}} + \phi_0 g_n^{\phi} \quad n = 1, 2, \ldots, N. \tag{36}$$

The energy flux of the nth reflected propagating mode and the total energy of all reflected propagating modes are given by Eqs. (24) and (25). For the present case of passive vibration control, the total energy of all reflected propagating modes from the amplitudes of Eq. (36) is

$$\mathscr{E}_{\mathrm{out}} = (a^{\mathrm{in}})^2 \chi_2 - a^{\mathrm{in}} \phi_0 \chi_1 + \phi_0^2 \chi_0, \tag{37}$$

where

$$\chi_0 = \sum_{n=1}^{N_{\mathrm{pr}}} \bar{g}_n^{\phi} g_n^{\phi} J_n, \quad \chi_1 = \sum_{n=1}^{N_{\mathrm{pr}}} (\bar{g}_n^{\phi} g_n^{\mathrm{in}} + g_n^{\phi} \bar{g}_n^{\mathrm{in}}) J_n, \quad \chi_2 = \sum_{n=1}^{N_{\mathrm{pr}}} \bar{g}_n^{\mathrm{in}} g_n^{\mathrm{in}} J_n. \tag{38}$$

Note that χ_0 and χ_2 are real and positive. It was also observed that χ_1 was positive in the range of frequencies considered. The extremum of $\mathscr{E}_{\mathrm{out}}$ is obtained by differentiating Eq. (37) with respect to ϕ_0 and setting the result to zero

$$\frac{\mathrm{d}\mathscr{E}_{\mathrm{out}}}{\mathrm{d}\phi_0} = 2\phi_0 \chi_0 - a^{\mathrm{in}} \chi_1 = 0 \rightarrow \phi_0 = \frac{\chi_1}{2\chi_0} a^{\mathrm{in}}. \tag{39}$$

Since χ_0 and χ_1 are both positive, the sign of ϕ_0 is positive, thus affirming the out-of-phase nature of end voltage with the incident wave. Thus, the total minimized energy flux is

$$\mathscr{E}_{\text{out}} = (a^{\text{in}})^2 \left[\chi_2 - \frac{\chi_1^2}{4\chi_0}\right]. \tag{40}$$

The following examples illustrate the effects of the applied voltage.

Example 3. For the homogeneous cylinder, let the incident wave be the lowest axisymmetric wave striking the traction-free end in the presence of an applied voltage, i.e.,

$$T_{zz} = T_{z\theta} = T_{zr} = 0, \quad \phi = \phi_0 v(r) \mathrm{e}^{-\mathrm{i}\omega t}, \tag{41}$$

where ϕ_0 is an unknown real constant and the voltage distribution is

$$v(r) = \begin{cases} -1, & 0.5 \leqslant r < 1, \\ +1, & 1 \leqslant r \leqslant 1.5. \end{cases} \tag{42}$$

In Fig. 10, the energies carried by the various outgoing propagating modes are plotted as a function of the incident wave frequency. Also, a curve for the total energy of all these outgoing waves is shown. Over the frequency range $1.5 \leqslant \omega \leqslant 4.5$, there are three frequencies at which there were relative maxima of incident wave energy collection (or harvesting), where the total energies of the outgoing waves were minima. At $\omega = 1.941$, 2.225 and 3.863, observe that 95.5%, 27.7% and 97.5% of the energy of the incident wave was collected leaving 4.5%, 72.3% and 2.5% to be shared by one, three and two possible outgoing waves, respectively.

Example 4. For the two-layer cylinder with the same conditions as Example 3, Fig. 11 shows the same type of data as Fig. 10. At $\omega = 1.88$, 23.5% of the incident wave energy was removed from the two possible out going waves. At $\omega = 3.864$, 96.7% of the incident wave energy was harvested, leaving only 3.7% to be shared by the three possible outgoing modes.

These two examples with a relatively simple voltage distribution given by Eq. (42) illustrate the amount of incident wave energy that can be extracted as a function of frequency. The locations of relative maximum energy harvests are seen. With another voltage distribution, relative maximum energy harvests will occur at other frequencies.

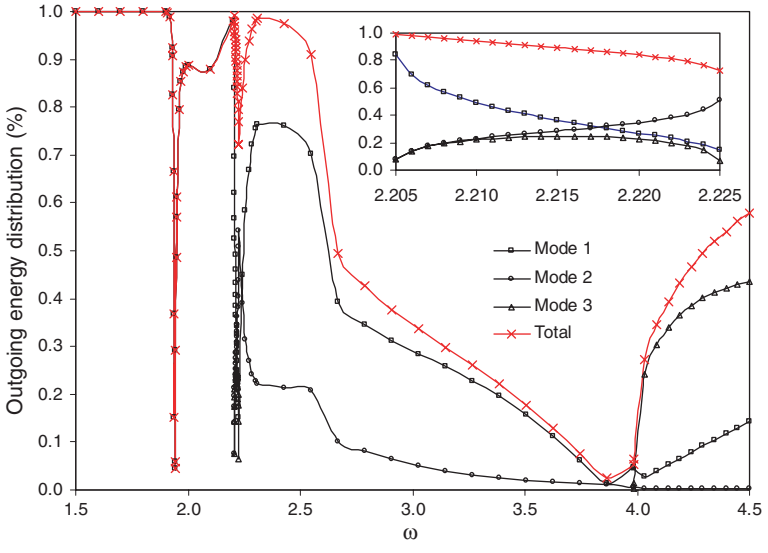

Fig. 10. Energy carried by reflected propagating waves with an oscillating voltage in homogeneous PZT4 cylinder.

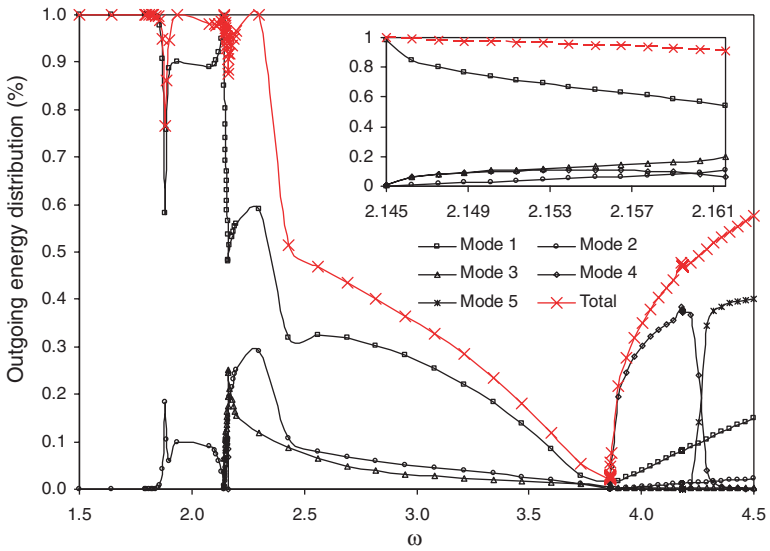

Fig. 11. Energy carried by reflected propagating waves with an oscillating voltage in two-layer PZT4 cylinder.

8. Conclusions

The reflected wave field in a layered piezoelectric cylinder is determined by a wave function expansion, whose coefficients can be determined by least-squares or virtual work. Both passive end reflection and forced motion by an oscillating voltage applied at the free end of the cylinder were considered.

End resonances were observed in both homogeneous and two-layer PZT-4 cylinders for axisymmetric incident waves at frequencies slightly below their first cutoff frequencies.

With an out-of-phase oscillating voltage on the end in the presence of the incident wave, energy can be extracted or harvested. Examples showing maximum energy harvest versus frequencies are given. Conceivably, different voltage distributions over an entire incident wave frequency range can be programmed to maximize energy extraction throughout this range.

References

Bai, H., Taciroglu, E., Dong, S.B., Shah, A.H., 2004. Elastodynamic Green's functions for a laminated piezoelectric cylinder. International Journal of Solids and Structures 41, 6335–6350.

Berlincourt, D.A., Curran, D.R., Jaffe, H., 1964. Piezoelectric and piezomagnetic materials and their function in transducers. Physical Acoustics 1 (Part A), 169–270.

Gregory, R.D., Gladwell, I., 1983. Axisymmetric waves in a semi-infinite elastic rod. Quarterly Journal of Mechanics and Applied Mathematics 42, 327–337.

Karunasena, W.M., Shah, A.H., Datta, S.K., 1991. Reflection of plane strain waves at the free edge of a laminated composite plate. International Journal of Solids and Structures 27 (8), 949–964.

Kim, Y.Y., Steele, C.R., 1989. End effects and time harmonic longitudinal wave propagation in a semi-infinite solid cylinder. ASME Journal of Applied Mechanics 56, 334–346.

McNiven, H.D., 1961. Extensional waves in a semi-infinite elastic rod. Journal of the Acoustical Society of America 33, 23–27.

Oliver, J., 1957. Elastic wave dispersion in a cylindrical rod by a wide-band short-duration pulse technique. Journal of the Acoustical Society of America 29, 189–194.

Rattanawangcharoenn, N., Shah, A.H., Datta, S.K., 1994. Reflection of waves at the free edge of a laminated circular cylinder. ASME Journal of Applied Mechanics 61, 323–329.

Siao, J.C.-T., Dong, S.B., Song, J., 1994. Frequency spectra of laminated piezoelectric cylinders. ASME Journal of Vibration and Acoustics 116, 364–370.

Taweel, H., Dong, S.B., Kazic, M., 2000. Wave reflection from the free end of a cylinder with an arbitrary cross-section. International Journal of Solids and Structures 37, 1701–1726.

Torvik, P.J., 1967. Reflection of wave trains in a semi-infinite plate. Journal of the Acoustical Society of America 41, 346–353.

Wu, C.H., Plunkett, R., 1972. On the solution of plates, strips, rods and cylinders subject to arbitrary dynamic edge load. SIAM Journal of Applied Mathematics 15, 107–119.

Zemanek, J., 1972. An experimental and theoretical investigation of elastic wave propagation in a cylinder. Journal of the Acoustical Society of America 51 (1), 265–283.